Digital Discovery

ROYAL SOCIETY OF CHEMISTRY

PAPER

View Article Online
View Journal

Cite this: DOI: 10.1039/d5dd00274e

Accelerated sol–gel synthesis of nanoporous silica *via* integrated small angle X-ray scattering with an open-source automation platform

Brenden Pelkie, Chi Yuet Yung, Zachery R. Wylie and Lilo D. Pozzo *

Received 20th June 2025
Accepted 1st September 2025

DOI: 10.1039/d5dd00274e

rsc.li/digitaldiscovery

Sol–gel syntheses can produce diverse arrays of nanomaterials, including mesoporous colloidal silica, within chemical design spaces that can become exceedingly large, complex, and expensive to explore *via* traditional methods. A new workflow for sol–gel automated synthesis of SiO_2, based on the open-hardware platform Science-Jubilee with integrated small angle X-ray scattering (SAXS), is demonstrated to outline correlations between precursor concentrations and morphological properties including particle size, polydispersity, extent of internal porosity and type of pore-phase order. Development of open and accessible high-throughput experimentation approaches is critical to accelerating the application of bespoke mesoporous silica nanostructures for potential use in chemical separations, catalysis, and drug delivery among other fields. The new hardware and workflow adapts and extends the Science-Jubilee automation platform for sol–gel synthesis and also integrates the NIST-design for the autonomous formulation laboratory (NIST-AFL) to achieve *in situ* structural characterization using either synchrotron and/or laboratory small-angle X-ray scattering (SAXS) instruments. An experimental campaign for SiO_2 room-temperature sol–gel synthesis using cetyltrimethylammonium bromide (CTAB) and Pluronic F127 surfactants, ammonia and tetraethyl orthosilicate (TEOS), demonstrates that it can reproducibly yield colloidal silica of variable size, dispersity, and internal pore phase order. The results also correlate well with published synthetic outcomes using traditional manual methods.

1. Introduction

Mesoporous and nanoporous colloidal silicas are synthesized *via* sol–gel methods that incorporate micelle-forming surfactants to produce an ordered (nano)porous internal structure. Mesoporous silicas are critical in a wide range of applications. In chemical separations, mesoporous silica chromatography column packings enable efficient separations due to their narrow particle and pore size distributions[1,2] and improve the performance of pervaporation separations when included in membranes.[3] Mesoporous silica nanoparticles (MSNs) are also promising drug delivery platforms. Pores can be loaded with pharmaceutical ingredients to circumvent limited drug solubility and other delivery issues,[4] and particle surfaces can also be functionalized to promote targeted delivery[5,6] and coated with stimuli-responsive coatings to control drug release.[7] Pore and particle size control is important to optimize delivery and release characteristics.[4,8] While drug delivery applications are still in development, mesoporous silica has been used for decades in tablet formulations as an excipient.[9] In catalysis, mesoporous silica can serve as a support substrate for metallic heterogeneous catalysts,[10] where the material's high specific surface area and controllable pore sizes contributes to high mass transfer and can prevent metal sintering.[11] MSN supported metallic catalysts have shown promising results for various CO_2 utilization reactions including CO_2 methanation,[12] CO_2 photoreduction[13] and electrocatalytic reduction of CO_2 with Ag or Au nanoparticles.[14]

Colloidal silica particles are typically synthesized through a surfactant templated sol–gel process illustrated in Fig. 1. In the traditional sol–gel synthesis, commonly referred to as the Stöber process,[15] a silicon alkoxide such as tetraethyl orthosilicate (TEOS) undergoes a base-catalyzed hydrolysis reaction (often using ammonia) followed by a condensation process to form nanoparticles. Mesoporous silica can be produced by including a micelle-forming surfactant, such as cetyltrimethylammonium bromide (CTAB), in the synthesis. The surfactant micelles provide a template for silicic acid monomers to condense around, before the resulting oligomer–micelle complexes aggregate and condense to form highly ordered porous structures.[16,17] The packing of the porous phase is thus controlled by the micelle structure and reaction conditions. The synthesis of a mesoporous silica material was first reported in 1992 with the development of the Mobil Composition of Matter (MCM) mesoporous silicas.[18] These materials were subsequently deployed commercially in 2002,[19] a notably fast development timeline for a novel material. Common pore phases for

Department of Chemical Engineering, University of Washington, Seattle, WA, USA. E-mail: dpozzo@uw.edu

these materials include the hexagonal rods of the canonical Mobil composition of matter (MCM)-41 (ref. 18) and Santa Barbara amorphous (SBA)-15 (ref. 20) mesoporous silicas, and the gyroid cubic packing of MCM-48.[18]

Several approaches to synthesizing mesoporous silicas have been investigated with the goal of gaining control over particle morphology and aggregation, pore size, and pore arrangement, including evaporation induced self assembly,[21] simple monophasic solution synthesis,[22] heterogeneous oil–water biphasic systems,[23] semi-batch continuous TEOS addition,[24] and other schemes.[25] This complex space of synthesis routes multiplies when the potential for including new surfactants as templates to control pore phase properties. Many of the reported mesoporous silica synthesis routes have been well characterized and the general factors that impact particle morphologies are understood in a 'directional' sense. For example, it is generally accepted that ammonia, TEOS concentration, and temperature control particle size,[26] and that surfactant chain length controls internal pore size.[16] However, these understandings are often stated as general trends, rather than prescriptive guidelines for achieving target mesoporous silica morphologies. Many studies do not quantify the reproducibility of their results and draw conclusions from single replicates. As Noureddine and coworkers hypothesize,[26] the complexity of synthesis methods present in the literature may hinder the adoption of MSNs for downstream applications, as selecting appropriate synthesis conditions to produce MSNs with specific target morphologies requires navigating a vast design space.

An automated synthesis and characterization procedure for mesoporous silica could help overcome these challenges by facilitating repeatable, high-throughput explorations of synthesis parameter space and enabling closed-loop optimization to discover appropriate synthesis conditions for target morphologies. Mesoporous silicas are well suited to study with a high-throughput or accelerated experimentation approach due to liquid-based, ambient-condition synthesis procedures, complex dependency of material morphologies on synthesis conditions, and large parameter space of compositions and component identities. In this work, we describe such a system for the automated synthesis and characterization of mesoporous materials. This system performs sol–gel synthesis with an open-source liquid handling platform and integrates with small-angle X-ray scattering (SAXS) instruments for sample characterization, as illustrated in Fig. 2. The Science-Jubilee open-hardware laboratory automation platform is used to automate the synthesis process[27,28] utilizing an adapted version of the 'Digital Pipette' syringe tool[29] to provide liquid handling capabilities. SAXS instruments, including a lab-scale facility and a synchrotron beamline, are used for sample characterization. A modified version of the NIST Autonomous Formulations Laboratory (AFL) sample loading module is used to automate sample loading from the Jubilee synthesis platform into the X-ray scattering instruments.[30] This platform enables the fully automated and reproducible synthesis of mesoporous colloidal silicas, allowing for high-throughput investigations and providing an important component of a self-driving lab for this material. Additionally, the use of open-source automation components showcases the promise of democratized approaches to accelerated experimentation.[31] This platform integrates three open-hardware automation components, including the internally co-developed Science-Jubilee and ones developed by the broader community (Digital Pipette and NIST-AFL). Using open hardware provides flexibility to meet the unique requirements of this sol–gel synthesis and facilitates extension of the platform by other researchers to study alternative sol–gel synthesized systems such as solid silica nanoparticles or other metal-oxide nanomaterials. The hardware and workflow described here complements other advancements in automated sol–gel synthesis, such as the automated nanomaterial self-driving lab reported by Zaki *et al.*[32]

SAXS is a powerful technique for the automated characterization of porous nanomaterials. X-ray scattering provides volume-averaged structural information over a broad range of length scales with a single instrument, from atomic crystalline structure (wide-angle X-ray scattering or X-ray diffraction) through mesopores (small-angle X-ray scattering or SAXS) to particle size, shape, and aggregation (ultra-small angle X-ray scattering or USAXS). Samples can be quickly (seconds to

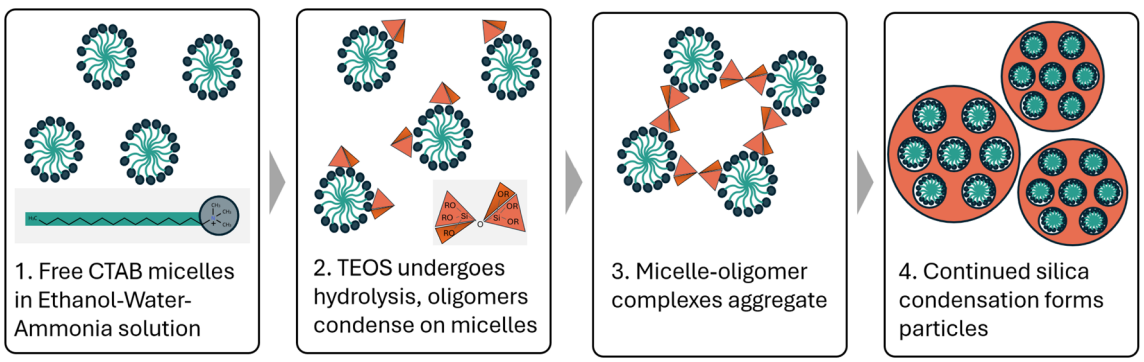

Fig. 1 Illustration of the cooperative assembly mechanism of particle formation during the synthesis process. (1) CTAB solution is added to a mixture of ethanol, water, and ammonia, resulting in free micelles. (2) TEOS is added to the micelle-containing solution. TEOS undergoes hydrolysis to form silicic acid monomers, which interact with the micelles. (3) Micelle-oligomer complexes aggregate to form assemblies. (4) Continued TEOS condensation produces spherical particles.

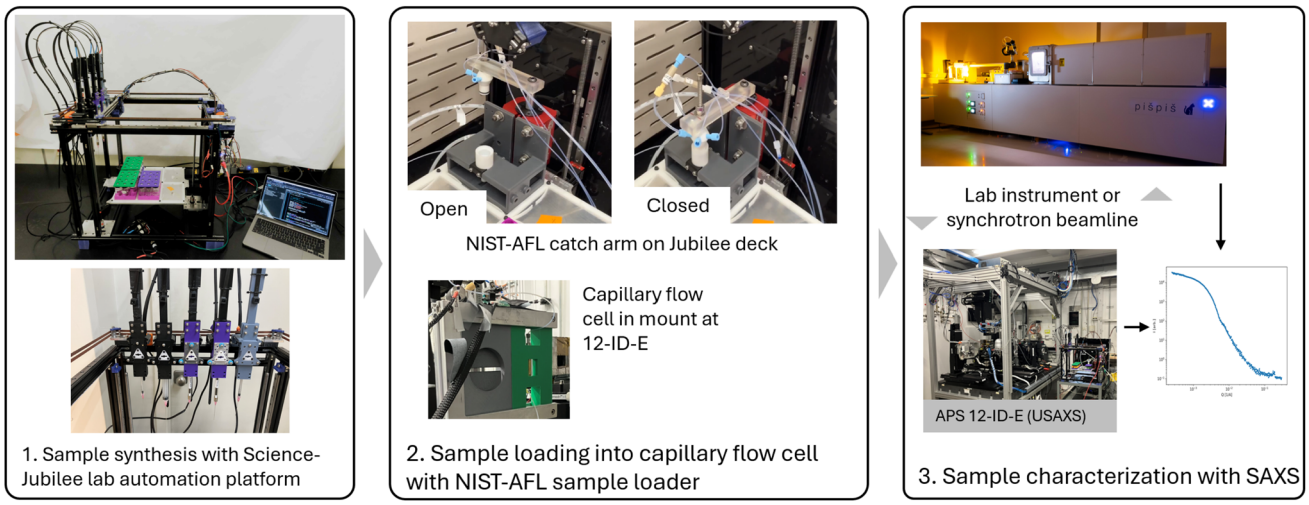

Fig. 2 Overview of automated synthesis platform. Colloidal silica samples are synthesized on Jubilee, transferred for characterization using the NIST-AFL sample loader, and characterized with small-angle X-ray scattering using either a laboratory instrument or synchrotron beamline.

minutes) measured as liquid dispersions, making the method amenable to automation.

The automated synthesis and characterization system described in this work was used to perform an initial composition space screening for a mesoporous colloidal silica synthesis. This synthesis campaign validates that the system is capable of reproducibly synthesizing monodisperse colloidal silicas with highly ordered mesoporous structures, supports insights into synthesis – morphology relationships for this system, and provides an initial starting point for future autonomous optimization campaigns. The binary surfactant mesoporous silica synthesis procedure first reported by Kim *et al.*[25] was used for this exploration. This procedure modifies the traditional Stöber synthesis by adding two surfactants: a cationic surfactant such as CTAB to serve as a pore template, and Pluronic F127 to aid in particle dispersity. It is performed at ambient conditions, can produce monodisperse, colloidally stable particles, and can be performed in around 20 minutes on the Jubilee platform, all of which make it amenable to automated and autonomous experimentation.

2. Materials and methods

2.1. Mesoporous colloidal silica synthesis

TEOS (Sigma Aldrich), anhydrous ethanol (Decon labs), CTAB (TCI), Pluronic F127 (Sigma), and ammonium hydroxide aqueous solution (Sigma) were all used as received. Ultra-pure water from a Millipore Direct-Q System (resistivity > 18 MΩ cm) was used throughout. The synthesis was performed on a Science-Jubilee laboratory automation platform. Science-Jubilee is an extension of the Jubilee open-hardware 3D printer project. The Science-Jubilee project extends the Jubilee open-hardware 3D printer project[28,33] to include tools, software, and documentation that facilitates laboratory automation.[27] Liquid handling for the sol–gel synthesis was performed with a modified implementation of the Digital Pipette liquid handling tool.[29] The 3D printed components of the tool were modified to integrate with the Jubilee tool changing mechanism, and the control software was adapted into the Science-Jubilee Python library. Five Digital Pipette tools were used in this synthesis procedure: a dedicated 1 cm^3 disposable plastic syringe dispensed water, dedicated 1 cm^3 glass syringes (Hamilton) dispensed TEOS and ammonium hydroxide solution, a shared 1 cm^3 disposable plastic syringe dispensed both aqueous CTAB and Pluronic F127 solutions, and a shared 10 cm^3 disposable plastic syringe dispensed ethanol, mixed samples, and transferred samples to the NIST-AFL sample loader (described below) for characterization. 1 cm^3 syringes provide more precision for low-volume transfers compared to 10 cm^3 syringes. Glass syringes were used with TEOS and ammonia due to incompatibility of these reactants with the plastic syringes. Accuracy for the used Digital Pipette tools is shown in SI Tables S3–S5. Documentation for the Science-Jubilee/Digital Pipette integration is available on the Science-Jubilee project website.[34] The Science-Jubilee was used with the lab automation deck component, which retains 6 standard SLAS labware plates in a grid.

Sample synthesis was performed in 20 mL glass scintillation vials. Custom 3D printed labware was used to hold the vials. A synthesis volume of 10 mL per sample was used. This synthesis involves volatile reactants – ammonium hydroxide solution and ethanol. Evaporation of these components needs to be prevented to avoid changes to sample compositions during synthesis. TEOS vapors are also hazardous, and mitigation is needed to limit exposure. Pre-slit silicone septa were used on all reaction and stock solution vials to minimize evaporation. This effectively prevented reactant evaporation and allowed for the synthesis procedure to be run outside of a fume hood, facilitating sample preparation at the beamline. The automated synthesis procedure was controlled from a Jupyter notebook using the Science-Jubilee Python package to control the Jubilee platform.[27]

Table 1 Composition bounds. Bounds for liquid components are reported as volume fraction of final sample mixture, while surfactant components are reported as concentrations in [mg mL^{-1}] in the final sample mixture

Component	Lower bound	Upper bound
TEOS	0.0035	0.04
Ammonium hydroxide solution	0.01	0.08
Ethanol	0.2	0.4
CTAB [mg mL^{-1}]	1	10
Pluronic F127 [mg mL^{-1}]	0	30
Water	0.3	1

2.2. Experimental design and workflow

For the batch synthesis campaign, a space filling experimental design strategy was used to select sample compositions. An experimental parameter space was selected by defining composition bounds on each component. Composition bounds (Table 1) were selected by expanding the compositions explored by Kim *et al.*[25] and identifying ranges likely to produce dispersed colloids through initial experiments. A set of randomly selected compositions from within these bounds was generated using a constrained Sobol rejection sampling strategy which selected samples that met the constraints imposed by the selected composition bounds and the necessity that all volume fractions sum to 1. First, a set of 128 composition values for the first five components (excluding water) was generated with a Sobol sequence.[35,36] For each sampled composition, the volume fraction of water required to meet the additive constraint was then calculated, accounting for water added during the addition of aqueous surfactant solutions. Compositions meeting all composition bound and additive constraints were retained, and the rest were discarded. This process was repeated until 80 valid sample compositions were selected. 63 of these selected samples were successfully synthesized within available time at a synchrotron beamline. Additionally, further experiments were run to validate the reproducibility of the synthesis protocol.

2.3. Synthesis execution

Stock solutions of TEOS, ammonium hydroxide solution, ethanol, water, CTAB solution (aqueous) and Pluronic F127 solution (aqueous) were prepared. TEOS was dissolved in ethanol at a ratio of 1 part TEOS:1.85 parts ethanol by volume. This dilution was necessary to increase the syringe delivery volume for TEOS dispensing, which increases the relative precision of low-volume dispenses. This dilution amount was selected such that the minimum dispense volume for the lower bound of the TEOS composition space would be 100 μL, which was identified as the minimum reasonable volume for precise transfers with the syringe tool (Table S4). CTAB was dissolved in water at a concentration of 15 g CTAB per liter of water. The mixture was lightly heated on a hot plate to dissolve. Recrystallization during the synthesis campaign was prevented by periodically re-heating the CTAB solution on the hot plate during synthesis campaigns. Pluronic F127 solution was prepared at a concentration of 50 g L^{-1} by dissolving Pluronic F127 powder in water. Ethanol, ammonium hydroxide solution, and water were used without preparation. Stock solutions were transferred to 20 mL septa-covered vials and placed on the Jubilee deck.

The actual delivery volume for each reactant was calculated from the target sample composition and the stock solution compositions. For example, the water delivered with the aqueous CTAB solution is accounted for in the total water delivered to the sample. A typical nanoparticle synthesis involves the following steps, which are also depicted in Fig. 3 and SI Video 1. (1) Ethanol is transferred from the ethanol stock vial to the sample vial using the 10 cm^3 syringe tool. (2) Water is dispensed into the sample vial from the dedicated 1 cm^3 water syringe tool. The syringe is refilled from the water stock vial as needed. (3) Ammonia solution is dispensed with the dedicated syringe tool. (4) CTAB solution is dispensed with the shared surfactant syringe, then the syringe is rinsed by aspirating and dispensing ethanol from a series of three rinse vials dedicated for use before TEOS is added to a sample. (5) Pluronic F127 solution is dispensed with the shared surfactant syringe, then the syringe is rinsed as it was after CTAB. (6) The precursor solution is mixed *via* aspirate/dispense cycles with the 10 cm^3 syringe used for ethanol. (7) TEOS is added with the dedicated syringe tool. The Jubilee immediately swaps for the 10 cm^3 syringe tool, then mixes the sample with aspirate/dispense cycles. (8) The 10 cm^3 syringe is rinsed in a series of 4 post-TEOS addition ethanol vials. (9) Particle growth is complete and the sample is ready to be loaded for measurement two hours after TEOS addition. The entire synthesis process takes approximately 20 minutes of active Jubilee time per sample.

This procedure performs mesoporous silica synthesis without requiring temperature control or continuous well plate stirring capabilities, which simplifies the implementation, and reduces hardware costs and complexity associated with integrating separate heating and stirring modules to the Science-Jubilee platform. Still, we note that the integration of standardized commercial modules is possible with the platform and that this would provide additional control to investigate transport and temperature effects, which have been found to be important in other sol–gel synthesis procedures.[37,38] Variations in reagent delivery protocols (*e.g.* all at once *vs.* timed delivery) are also possible to implement and to investigate with simple modifications to the existing code. Such variations in procedures can be implemented on Science-Jubilee *via* commercial or open-source modules (*e.g.* magnetic stirring and/or heating) on the labware deck and by altering the control procedures. The possible variations in protocols and hardware configurations are vast and need to be carefully scoped for specific synthesis questions. The open-source nature of the platform supports the addition of these and new capabilities to enable studies of various synthesis procedures.

2.4. Sample transfer to characterization instruments

The NIST-AFL sample loading system was used to transfer samples from the Jubilee synthesis platform to X-ray scattering

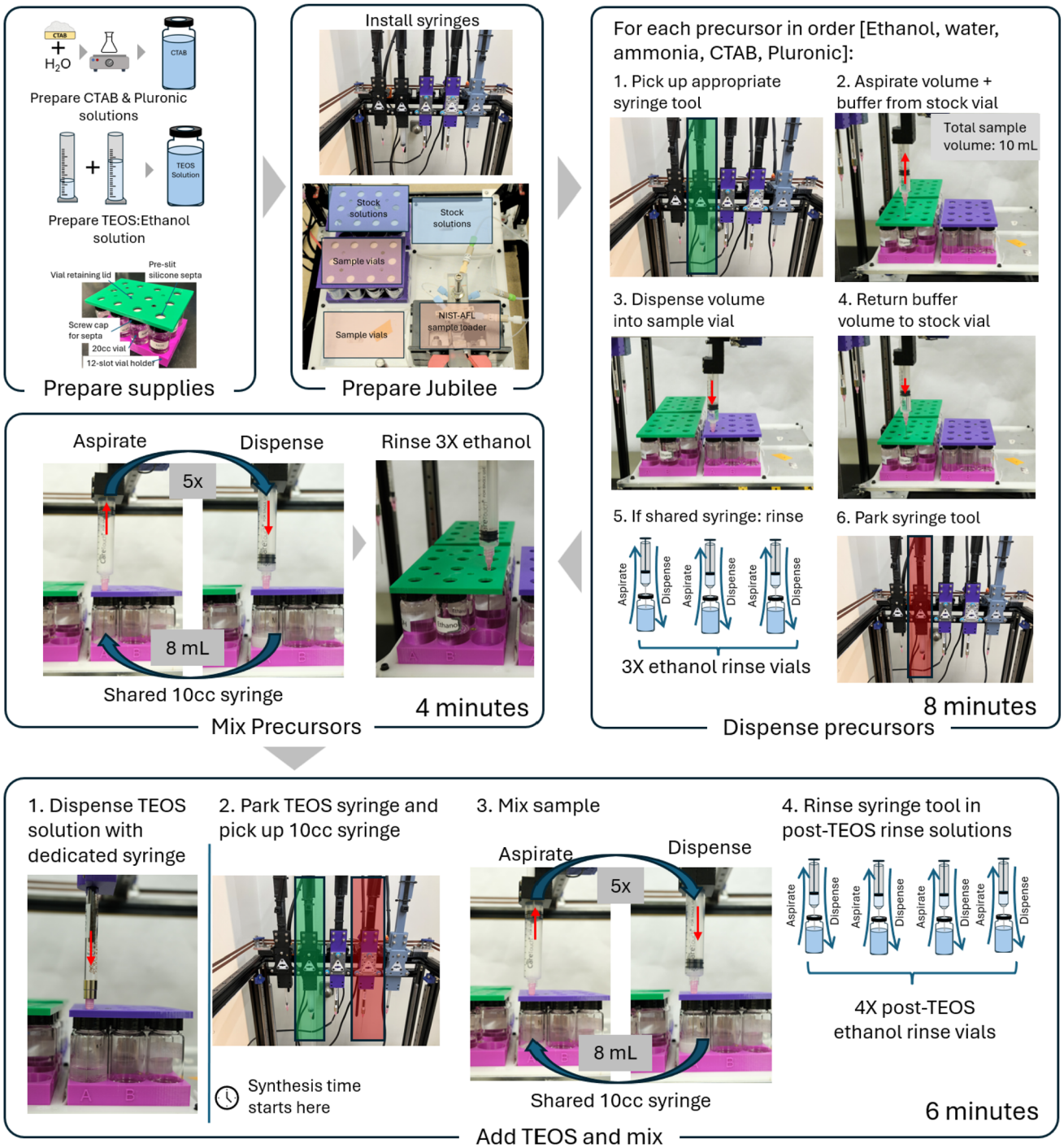

Fig. 3 Mesoporous colloidal silica synthesis protocol. Synthesis components are first manually prepared and loaded onto the Jubilee platform. The Jubilee system dispenses precursors into a reaction vial, mixes them using syringe aspirate–dispense cycles, then adds TEOS and mixes the sample to complete the synthesis.

instruments for sample characterization. The sample loader is a component of the NIST-AFL platform, an open-source initiative to develop autonomous experimentation capabilities for formulation development tasks.[30] The sample loader is a pneumatic system that uses air pressure to push a sample through flexible tubing into a quartz capillary flow cell (SI Fig. S10). To load a sample, the Jubilee robot transfers a sample into the NIST-AFL 'catch' cell using the 10 cm^3 mixing syringe tool. The catch cell is closed with a rotating clamp arm. Air pressure is used to move the sample through tubing until it reaches a capillary flow cell positioned in the X-ray instrument. After measurement, the sample contact path is rinsed and dried. More information on our implementation of this system for Jubilee can be found on the project GitHub repository, and

additional information on the NIST-AFL system can be found in the hardware and software repositories for this project.[39,40] The sample loader design used in this work is an update to the version described in the original AFL publication. The sample loader is well suited to run in a sequential one-sample-at-a-time mode. Alternatively, custom liquid cartridge cells were also used to run samples in a 'batch' mode. Documentation to reproduce these cells is available online.[41]

2.5. Small-angle X-ray scattering

Small-angle X-ray scattering (SAXS) measurements were made at the 12-ID-E USAXS beamline at the Advanced Photon Source,[42] and with a laboratory SAXS instrument. The USAXS instrument enables observation of larger structural features than the laboratory instrument, while the laboratory instrument provides higher resolution data at the high-q regions corresponding to scattering from the internal porosity of mesoporous samples. USAXS measurements were made with an X-ray energy of 21 keV ($\lambda = 0.5895$ Å). USAXS flyscan data were reduced and corrected using Igor. Data were corrected for instrumental and empty container background scattering and de-smeared to correct for instrumental slit smearing. Laboratory SAXS measurements were made using a Xenocs Xeuss 3.0 instrument with a Cu-Kα source ($\lambda = 1.5406$ Å). Data were reduced and corrected for empty container background scattering using XSACT 2.10 from Xenocs.

Operating this system in a fully automated manner requires integrating with X-ray scattering instruments to trigger measurements and collect completed data. This integration is instrument-specific due to varied sample mounting stages and control interfaces. Mechanically integrating the synthesis system with an instrument requires mounting the capillary flow cell and NIST-AFL electronic components on the instrument sample stage. This can be achieved with appropriate sample stages or custom 3D printed holders,[43] and requires the Science-Jubilee and NIST-AFL control hardware to be located next to the instrument. Software integration with the instrument control system is needed to trigger a measurement once a sample is loaded. The details of this implementation are instrument-specific, but common instrument control software including Bluesky and SPEC provide provisions for initiating measurements through a network request. The integrations developed in this work for the 12-ID-E and the Xenocs instrument are documented in the project GitHub repository.[44]

Raw X-ray scattering data also needs to be corrected, reduced and analyzed before it can be used to understand the structure of the sample it was generated from. For closed-loop autonomous experimentation, this data processing workflow needs to be automated to allow for fully autonomous optimization. Instrument-specific data reduction and correction processes perform the necessary transformations to convert raw detector data into 1-dimensional, intensity *vs.* scattering vector (q) data. Fully automated reduction and correction pipelines exist for many instruments, making it straightforward to attain reduced 1D data from a measurement. The larger challenge in integrating SAXS characterization into autonomous experiments is automation of the data analysis and interpretation process. This process traditionally requires extensive researcher involvement because it relies on external or *a priori* information about the sample and expert model selection. Nevertheless, the scattering community is making significant progress in developing methods to automate this process. Possible approaches include machine-learning classifier guided model fitting,[45–47] domain-specific structural solvers such as CREASE,[48,49] and shape-metric approaches to compare measured and target scattering.[50] While this problem is not addressed in this work, continued progress by us and by the broader community is expected to enable SAXS integration into autonomous experimentation workflows in the near future.

2.6. Dynamic light scattering

Dynamic light scattering (DLS) was used to measure particle sizes in initial exploratory and reproducibility verification campaigns. DLS measurements were made with a Malvern Instruments Zetasizer Nano ZS fitted with a 633 nm laser. As-prepared samples were diluted in water before measurements. Analysis was performed with Malvern Zetasizer Software version 8.0. Z-average diameters and PDI are reported here.

2.7. Electron microscopy

Scanning electron and transmission electron micrographs were collected from samples supported on a carbon grid. SEM images were collected on a Thermo Fisher Scientific Phenom Pharos desktop instrument in secondary electron detector mode operated at 20 kV. Samples were prepared for SEM by dispersing as-prepared samples in ethanol then drop-casting them on the grid. Transmission electron microscopy (TEM) was performed using a Tecnai G2 F20 SuperTwin TEM at an operating voltage of 200 kV using a Gatan Ultrascan CCD digital camera. TEM samples were first washed to remove surfactant using an acid wash procedure.[26] Washed samples were dispersed in ethanol and drop-cast onto grids.

3. Results and discussion

3.1. Workflow validation

Two assessments were used to understand the reproducibility of the automated synthesis workflow. In the first, a sample composition observed to produce highly monodisperse, colloidally stable (non-aggregating) particles was replicated. Sample 1 (composition listed in Table 2) was selected. This sample was replicated five times in a single synthesis run. Particle size was measured with DLS, and the mesoporous structure was characterized with SAXS. Across the five samples, the particle diameters were similar (average particle diameter 778 nm, with a standard deviation of 12 nm), and the scattering data from the mesoporous region is nearly identical for all particles (SI Fig. S1). These results suggest that the synthesis workflow is capable of reproducibly synthesizing samples.

In the second reproducibility check, control samples were synthesized throughout the main batch synthesis experiment (described below). Samples with identical compositions were

Table 2 Compositions of selected samples

Sample	TEOS vol. frac.	Ammonia vol. frac.	Ethanol vol. frac.	[CTAB] [mg mL^{-1}]	[F127] [mg mL^{-1}]	Water vol. frac.
1	0.008	0.018	0.37	5.0	6.9	0.60
2	0.019	0.064	0.21	2.8	6.3	0.70
3	0.034	0.055	0.21	7.5	0.5	0.70
4	0.029	0.022	0.23	4.2	5.3	0.72
5	0.011	0.059	0.29	5.4	1.8	0.64
6	0.007	0.021	0.40	7.0	1.0	0.57

made in triplicate at the start of the experiment, then at regular intervals of approximately 25 samples or 8.5 hours over the course of the 24 hours synthesis campaign. The control composition was selected as the most monodisperse sample from early exploratory experiments and is shown in SI Table S1. The scattering data suggests all samples were polydisperse in diameter. While samples 1–4 were well dispersed, the scattering for sample 5 suggests particle aggregation (SI Fig. S2). Additionally, the high-Q scattering of sample 2 suggests a different internal porous structure than the other four samples. These results suggest that both internal porous structure and colloidal stability were identical in four out of five samples over a 24 hours campaign. Discrepancies could be due to small variations in the delivered volume from the syringe tool that could cause slightly different sample compositions. Such variations in mechanical devices are present in any automated or 'manual' synthesis system or protocol, and it is important to systematically quantify them to assess reproducibility of any given workflow.

Initial development experiments indicated that effective control of ammonia evaporation is important for achieving reproducibility in this synthesis as ammonia concentration has a large influence over particle size and ammonia is highly volatile. Researchers working on similar sol–gel syntheses, whether using automated systems or traditional manual methods, should take precautions to prevent ammonia concentration changes due to evaporation from impacting results. In this work, silicone septa were used to minimize evaporation.

Many reports also suggest that continuous stirring of the reaction mixture during and after TEOS addition is an important factor in determining the packing structure of the porous mesophase and potentially particle size.[25,51] The synthesis procedure presented in this work, however, replaces continuous stirring with repeated syringe aspirate/dispense cycles performed after reagent additions. To evaluate the impact of this procedural adaptation on sample morphologies, samples with identical compositions were synthesized using both magnetic stirring and the syringe mixing used here. The composition of sample 1 (Table 2) was used for this test. For the magnetically stirred samples, the precursor mixture (including all components except TEOS) was prepared on the Jubilee platform as discussed before, then TEOS was added with a manual pipette while stirring at 1000 RPM on a magnetic stir plate. Stirring was continued for 1 minute after TEOS addition, then stopped. This synthesis follows the procedure reported by Kim *et al.*[25] on which the synthesis studied in this work is based. The Jubilee syringe mixed samples were prepared following the general procedure presented in this work. Samples were characterized with dynamic light scattering to measure particle size and SAXS to compare mesopore phase structure. The resulting sizes were similar between methods (726 ± 45 nm for stirred, 778 ± 12 nm for jubilee, $n = 5$), and scattering from the porous structures was essentially identical (disordered porous structure, SI Fig. S1). This suggests that particles synthesized using this automated synthesis procedure are similar to those prepared made with manual synthesis procedure from which the automated protocol was developed.

3.2. Exploration of the design space for mesoporous silica nanoparticles

The automated synthesis platform was used to perform a batch parameter space exploration campaign. This experiment was performed at the APS 12-ID-E beamline. 63 samples were synthesized in the available experiment time from the 80 compositions generated with the constrained Sobol sampling method discussed above. Samples were continuously synthesized over a contiguous 24 hours period. Samples were characterized with USAXS using the custom liquid cartridge plates described in the methods section. Fully automated synthesis-characterization integration was achieved at 12-ID-E, and several samples were synthesized in this manner. However, the samples described here were prepared offline and measured in batch mode to more efficiently utilize time-limited beamtime for the initial screening experiment. A minimum of two hours elapsed between sample synthesis and USAXS measurement, which ensured complete reaction and stable synthesis (SI Fig. S13). To supplement the USAXS scattering data, additional SAXS data was collected from the same samples 11 days after synthesis on the Xenocs Xeuss 3.0 instrument to characterize the internal pore structure. SEM and TEM images of selected samples were also collected 26–60 days after sample synthesis.

Particle dispersion and size monodispersity are both important sample characteristics. This experiment campaign demonstrates that the automated synthesis presented is capable of producing stable, monodisperse particles, and that USAXS is an effective method for understanding these properties for colloidal silica samples in high throughput. Fig. 4 presents USAXS scattering data from four selected samples. SEM images of these samples are also shown. The scattering data presented in Fig. 4a suggests a sample consisting of

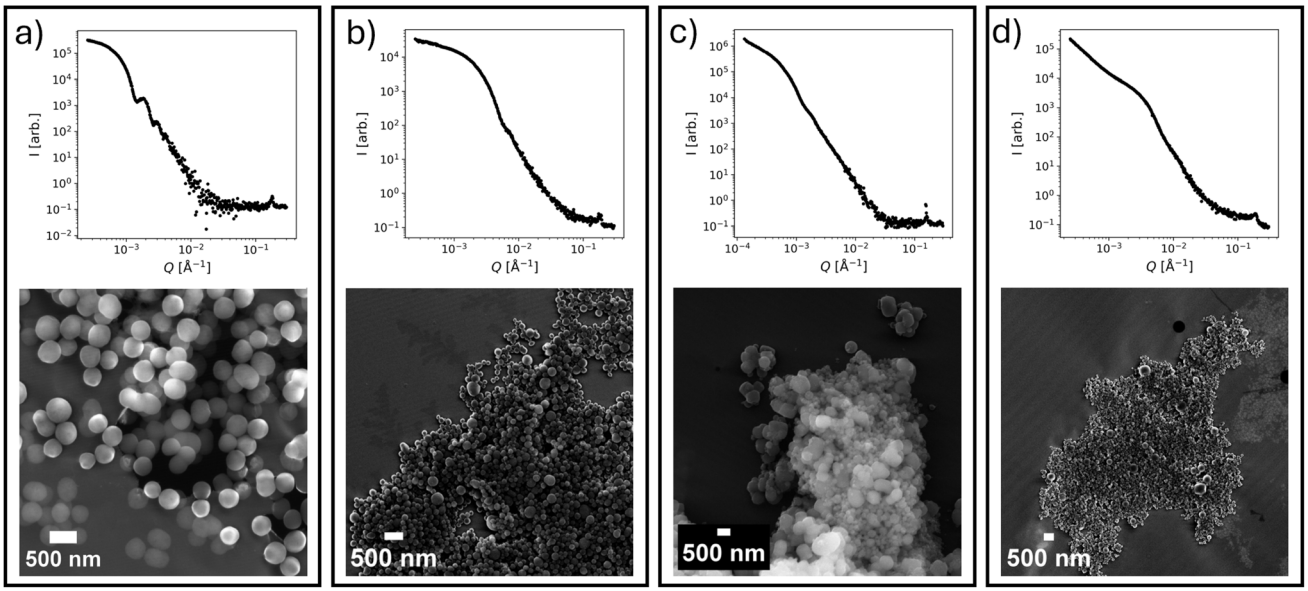

Fig. 4 SEM images and USAXS scattering for selected samples. (a) highly monodisperse sample (sample composition 1), (b) Moderately monodisperse sample (sample composition 2), (c) aggregated polydisperse sample (sample composition 3), and (d) aggregated polydisperse sample (sample composition 4).

monodisperse particles with minimal aggregation. Size monodispersity is indicated by the oscillations present in the intensity (y axis) as a function of Q (x axis), and minimal aggregation is indicated by the Guinier turnover to a flat slope at low Q values (left side of plot). The associated SEM image confirms that this sample contains uniformly sized, spherical particles with minimal aggregation. A polydisperse sphere model fit of the USAXS data suggests particles with a mean diameter of 602 nm (SI Fig. S3). Fig. 4b–d show samples whose scattering data suggests varying degrees of aggregation and polydispersity. The SEM images of these samples indeed confirm polydisperse, aggregated particles.

6 out of the 63 synthesized samples have USAXS scattering data that is consistent with stable, size monodisperse particles. Polydisperse sphere model fits made with the Sasview software[52] indicate that the mean diameters of these samples range from 220 nm to 630 nm, and that their associated polydispersity indices range from 0.08 to 0.19. Model fits are shown in SI Fig. S3–S8.

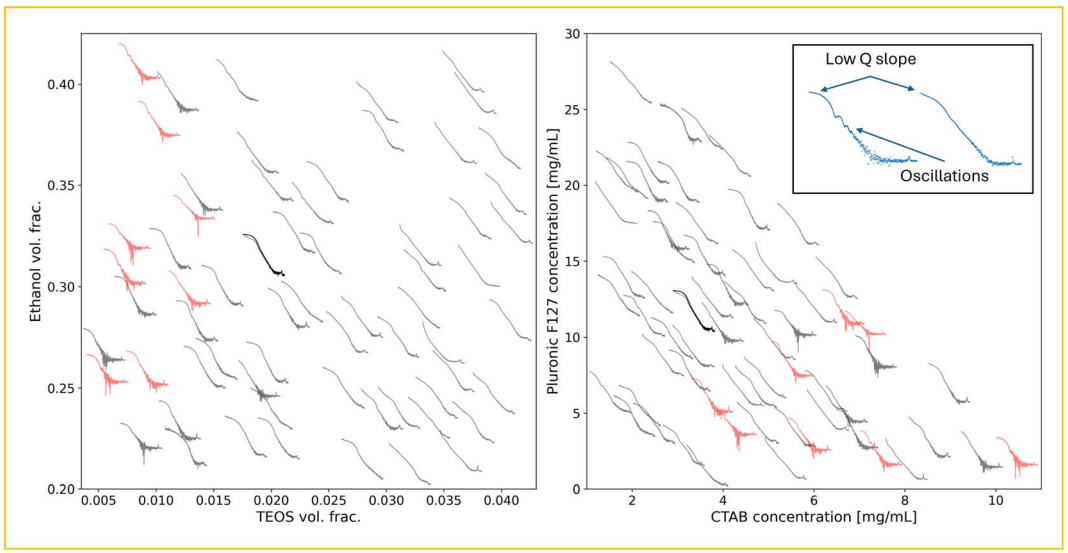

Fig. 5 Composition-scattering plots for USAXS scattering data demonstrates relationships between composition and particle morphology. USAXS scattering data for each sample is plotted at a position corresponding to that sample's composition with respect to the components in each axis. The inset highlights distinct features in the scattering data. Scattering from highly size monodisperse samples has clear oscillations while polydisperse samples lack this feature. Scattering from aggregated samples has a negative slope in the low-Q region (the left portion of the scattering data) while stable samples have a 'flat' region corresponding to the expected Guinier scattering behavior. Scattering qualitatively identified to demonstrate colloidally stable, monodisperse samples is highlighted in red.

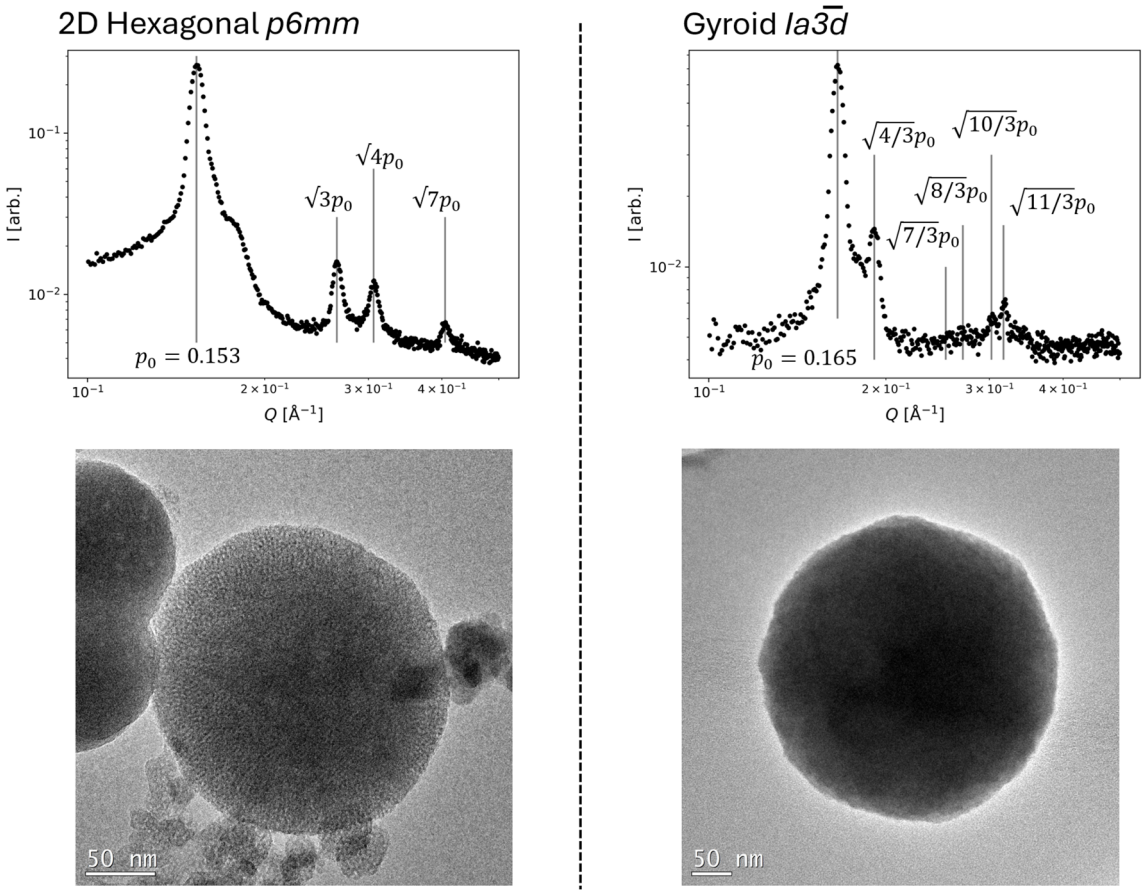

Fig. 6 Examples of samples exhibiting ordered 2D hexagonal (Sample 3) and gyroid (Sample 5) internal pore orderings. Internal porosity is visible in a TEM image of the hexagonal sample but cannot be seen in the gyroid sample.

The influence of sample composition on particle size monodispersity can be evaluated qualitatively. Fig. 5 presents the relationship between sample composition and USAXS scattering by plotting the measured scattering data directly in the composition space. Sample compositions low in TEOS, high in ethanol, and low in F127 favor monodisperse particles.

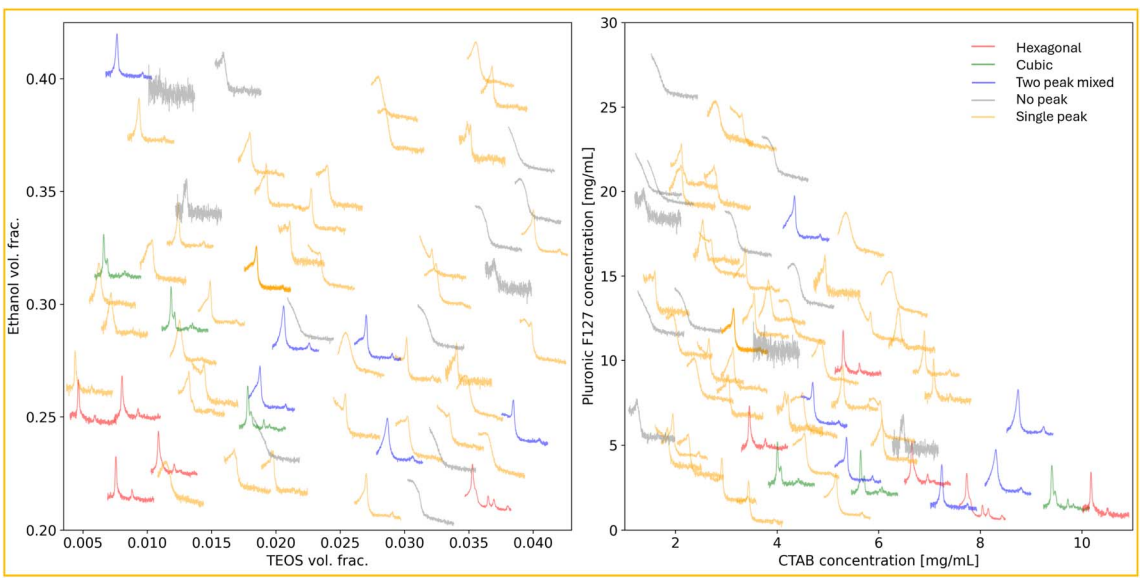

Fig. 7 Composition-scattering plots for SAXS measurements of samples. This plot is analogous to Fig. 5 but shows high-Q scattering associated with porous phase order from the same samples. Individual sample scattering is colored according to the identified internal pore phase.

Monodisperse scattering data is primarily present in the lower left corner of the composition-scattering plots, indicating low reagent concentrations. This campaign did not generate enough monodisperse samples to facilitate quantitative conclusions about composition – diameter relationships. Composition-aggregation relations can also be inferred from these plots by comparing the low-Q slope of the scattering data. Stable particles are produced primarily from samples with low TEOS content. Other components do not significantly impact aggregation.

Samples with a variety of ordered internal pore mesophases were formed, including those with hexagonal *p6mm* and gyroid $Ia\bar{3}d$ cubic structures. These phases were identified by multiple sharp peaks that index to known peak spacings.[53] Additionally, many samples exhibit an unidentified two-peak mixed phase, and others show a single, often broad peak suggesting poorly ordered pores. Fig. 6 shows examples of scattering from samples with ordered internal porous phases, along with TEM images showing their internal porous structure. Several samples do not have any high-Q scattering peaks, suggesting a lack of ordered pore formation.

Qualitative composition – structure relationships for pore ordering can also be investigated with composition-scattering plots (Fig. 7). These plots show that high CTAB content is necessary to form ordered mesoporous phases, which is expected given CTAB's role as the micelle-forming template surfactant in this system. Low Pluronic F127 content also favors ordered pore phase formation. We hypothesize that high Pluronic F127 content may interfere with CTAB micelle formation to inhibit mesoporous structure growth. Pluronic F127 was originally included in this synthesis to minimize particle aggregation.[25] However, stable samples were synthesized with low Pluronic F127 content, suggesting that this may not be a necessary component of the system, or that the selected upper composition bound for this experiment needs to be lowered. Low ethanol and TEOS content with moderate to high ammonia content and high water content also favors highly ordered pore phases. These qualitative conclusions are supported by a SHAP feature importance analysis applied to a peak sharpness score, more details of which are found in the SI. Fig. 7 also suggests a compositional dependence for phase selection. In particular, the ethanol-TEOS panel suggests that, as ethanol and TEOS compositions are jointly increased, the porous phase arrangement undergoes transitions from hexagonal to gyroid to 2-peak mixed to disordered phases.

Comparing the composition–morphology relationships for overall particle morphology and pore phase order suggests the existence of a trade-off between compositions that generate monodisperse, stable (non-aggregated) particles, and those that generate highly ordered internal pore phases. For example, a high ethanol content supports monodisperse particles, but a low content is associated with ordered pore phases. This effect can be observed in Fig. 8, which plots USAXS and SAXS data for examples of highly monodisperse samples as highly pore-ordered samples. This shows that the observed monodisperse samples have moderate pore ordering, while the highly ordered samples have at best moderate polydispersity. This suggests

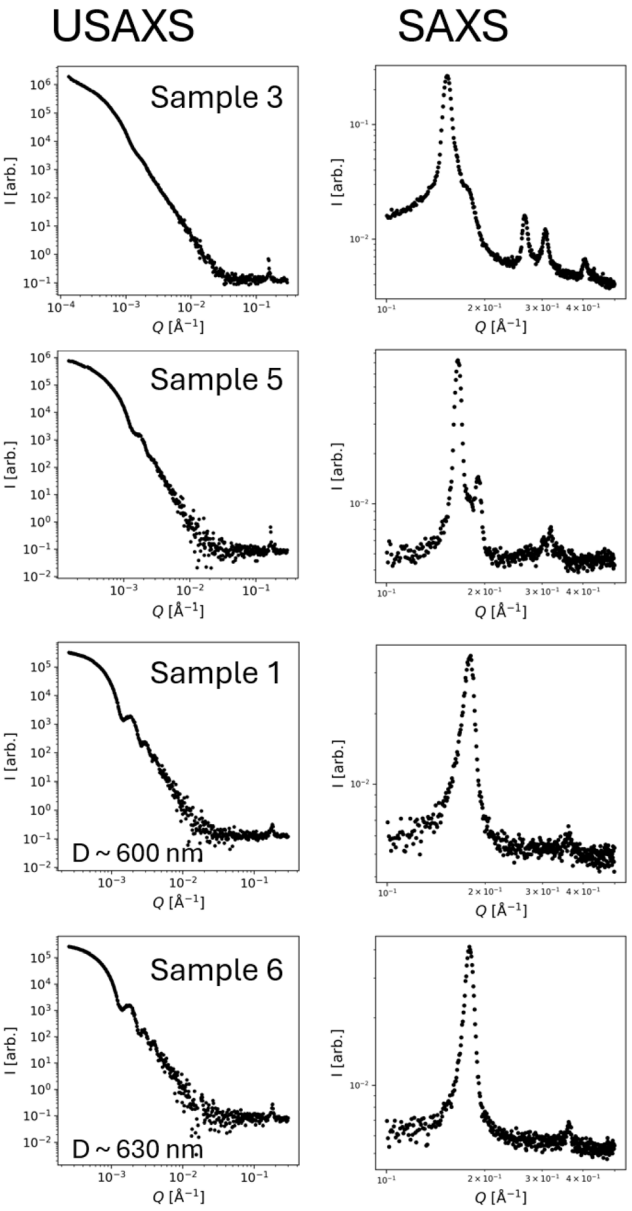

Fig. 8 The most monodisperse samples observed have poorly ordered porous phases, and the most ordered porous phase samples observed occur in polydisperse to moderately monodisperse particles. However, moderate monodispersity in Sample 5 suggests further optimization may yield monodisperse, highly ordered particles.

that further investigation, potentially with an autonomous optimization approach, would be necessary to identify compositions supporting both high diameter monodispersity as well as highly ordered pore phases.

4. Conclusions

An integrated automated synthesis and SAXS characterization system was developed and used for sol–gel nanomaterial synthesis. It is then used in a campaign to study correlations between the precursor composition space and the resulting morphology for mesoporous colloidal silica synthesis

procedures performed at room temperatures. This study demonstrated that the newly developed open-source platform is capable of synthesizing mesoporous silica particles with a wide range of particle sizes, dispersity, and internal ordered pore structures. This work also shows that SAXS and USAXS are effective and fast characterization methods for integrated automated sol–gel synthesis experiments.

This system and the initial exploratory dataset described in this work will enable future research to understand and optimize synthesis conditions for mesoporous colloidal silica and other sol–gel synthesized nanomaterials. The initial exploration conducted here will allow further investigations to study 'interesting' parameter spaces with active learning approaches. Possible objectives include phase boundary mapping to develop a better understanding of the conditions that lead to specific pore phase ordering, and morphology optimization to discover synthesis conditions for size monodisperse, colloidally stable particles with targeted particle sizes and pore structures. Many opportunities exist to expand on the synthesis conditions investigated here, for example by incorporating additional surfactants or adding a reaction quenching step to the synthesis. Our hope is also that other researchers adapt and extend this platform to accelerate research across a diverse range of sol–gel chemistries beyond the colloidal silicas studied here. The open-hardware nature of this system and available documentation make it possible for researchers to explore new synthesis steps and conditions or alternative characterization techniques by building off the existing capabilities discussed here. This integration of new accelerated experimentation methods with traditional sol–gel synthesis techniques will yield exciting advancements in nanomaterials development.

Author contributions

BP: hardware and software, investigation, data curation, visualization, writing – original draft and editing. CYY: hardware, investigation. ZRW: investigation. LDP: supervision, funding acquisition, writing – review and editing.

Conflicts of interest

The authors have no conflicts to declare.

Data availability

Additional information is available in the SI. Complete experiment information, data and code is available in an associated Zenodo repository **https://doi.org/10.5281/zenodo.16994907** and *via* GitHub at **https://github.com/pozzo-research-group/automated-mesoporous-silica**, including detailed procedures used to execute the experiments described here and resulting X-ray scattering data. Extensive hardware documentation for the Science-Jubilee project is available at **https://science-jubilee.readthedocs.io/en/latest/**, and the NIST-AFL implementation described here is documented at **https://github.com/pozzo-research-group/AFL-sample-loader**.

Supplementary information is available. See DOI: **https://doi.org/10.1039/d5dd00274e**.

Acknowledgements

The authors wish to thank Dr Peter Beaucage and Dr Tyler Martin for assistance with building the NIST-AFL sample loading system and integrating it at the Advanced Photon Source. Kiran Vaddi provided code to produce the composition-scattering plots (Fig. 5 and 7). Illustrations generated by Maria Politi were used in figures. This work was primarily supported by the AI-Core of the University of Washington Molecular Engineering Materials Center, an NSF MRSEC supported under award number DMR-2308979. The authors also acknowledge the use of SAXS facilities and instrumentation supported by the U.S. National Science Foundation through the Major Research Instrumentation (MRI) program DMR-2116265. This research was also performed on APS beam time award 10.46936/APS-188896/60013388 from the Advanced Photon Source, a U.S. Department of Energy (DOE) Office of Science user facility operated for the DOE Office of Science by Argonne National Laboratory under Contract No. DE-AC02-06CH11357. The authors acknowledge the use of facilities and instrumentation supported by the Molecular Analysis Facility, which is supported in part by funds from the Molecular Engineering & Sciences Institute, the Clean Energy Institute, and the National Science Foundation (NNCI-2025489 and NNCI-1542101). This work benefited from the use of the SasView application, originally developed under NSF award DMR-0520547. SasView contains code developed with funding from the European Union's Horizon 2020 research and innovation program under the SINE2020 project, grant agreement No. 654000.

References

1 D. Wang, X. Chen, J. Feng and M. Sun, Recent Advances of Ordered Mesoporous Silica Materials for Solid-Phase Extraction, *J. Chromatogr. A*, 2022, **1675**, 463157, DOI: **10.1016/j.chroma.2022.463157**.

2 K. W. Gallis, J. T. Araujo, K. J. Duff, J. G. Moore and C. C. Landry, The Use of Mesoporous Silica in Liquid Chromatography, *Adv. Mater.*, 1999, **11**(17), 1452–1455, DOI: **10.1002/(SICI)1521-4095(199912)11:17%253C1452::AID-ADMA1452%253E3.0.CO;2-R**.

3 E. J. Flynn, D. A. Keane, P. M. Tabari and M. A. Morris, Pervaporation Performance Enhancement through the Incorporation of Mesoporous Silica Spheres into PVA Membranes, *Sep. Purif. Technol.*, 2013, **118**, 73–80, DOI: **10.1016/j.seppur.2013.06.034**.

4 M. Vallet-Regí, F. Schüth, D. Lozano, M. Colilla and M. Manzano, Engineering Mesoporous Silica Nanoparticles for Drug Delivery: Where Are We after Two Decades?, *Chem. Soc. Rev.*, 2022, **51**(13), 5365–5451, DOI: **10.1039/D1CS00659B**.

5 V. López, M. R. Villegas, V. Rodríguez, G. Villaverde, D. Lozano, A. Baeza and M. Vallet-Regí, Janus Mesoporous Silica Nanoparticles for Dual Targeting of Tumor Cells and

Mitochondria, *ACS Appl. Mater. Interfaces*, 2017, **9**(32), 26697–26706, DOI: 10.1021/acsami.7b06906.

6 L. Xiong, X. Du, F. Kleitz and S. Z. Qiao, Cancer-Cell-Specific Nuclear-Targeted Drug Delivery by Dual-Ligand-Modified Mesoporous Silica Nanoparticles, *Small Weinh. Bergstr. Ger.*, 2015, **11**(44), 5919–5926, DOI: 10.1002/smll.201501056.

7 C.-Y. Lai, B. G. Trewyn, D. M. Jeftinija, K. Jeftinija, S. Xu, S. Jeftinija and V. S.-Y. Lin, A Mesoporous Silica Nanosphere-Based Carrier System with Chemically Removable CdS Nanoparticle Caps for Stimuli-Responsive Controlled Release of Neurotransmitters and Drug Molecules, *J. Am. Chem. Soc.*, 2003, **125**(15), 4451–4459, DOI: 10.1021/ja028650l.

8 M. Bouchoucha, M.-F. Côté, R. C. Gaudreault, M.-A. Fortin and F. Kleitz, Size-Controlled Functionalized Mesoporous Silica Nanoparticles for Tunable Drug Release and Enhanced Anti-Tumoral Activity, *Chem. Mater.*, 2016, **28**(12), 4243–4258, DOI: 10.1021/acs.chemmater.6b00877.

9 Excipients, https://grace.com/industries/pharmaceutical-solutions/purification-formulation-delivery/excipients/, https://grace.com/industries/pharmaceutical-solutions/purification-formulation-delivery/excipients/, (accessed 2025-05-06).

10 A. Mohan, A. Jaison and Y.-C. Lee, Emerging Trends in Mesoporous Silica Nanoparticle-Based Catalysts for CO2 Utilization Reactions, *Inorg. Chem. Front.*, 2023, **10**(11), 3171–3194, DOI: 10.1039/D3QI00378G.

11 X. Yu, T. Williams and C. Recent, Advances in the Applications of Mesoporous Silica in Heterogeneous Catalysis, *Catal. Sci. Technol.*, 2022, **12**(19), 5765–5794, DOI: 10.1039/D2CY00001F.

12 X. Wang, L. Zhu, Y. Zhuo, Y. Zhu and S. Wang, Enhancement of CO2 Methanation over La-Modified Ni/SBA-15 Catalysts Prepared by Different Doping Methods, *ACS Sustain. Chem. Eng.*, 2019, **7**(17), 14647–14660, DOI: 10.1021/acssuschemeng.9b02563.

13 X. Wang, X. Xuan, Y. Wang, X. Li, H. Huang, X. Zhang and X. Du, Nano-Au-Modified TiO2 Grown on Dendritic Porous Silica Particles for Enhanced CO2 Photoreduction, *Microporous Mesoporous Mater.*, 2021, **310**, 110635, DOI: 10.1016/j.micromeso.2020.110635.

14 M. Pal and V. Ganesan, Zinc Phthalocyanine and Silver/Gold Nanoparticles Incorporated MCM-41 Type Materials as Electrode Modifiers, *Langmuir*, 2009, **25**(22), 13264–13272, DOI: 10.1021/la901792b.

15 W. Stöber, A. Fink and E. Bohn, Controlled Growth of Monodisperse Silica Spheres in the Micron Size Range, *J. Colloid Interface Sci.*, 1968, **26**(1), 62–69, DOI: 10.1016/0021-9797(68)90272-5.

16 R. Narayan, U. Y. Nayak, A. M. Raichur and S. Garg, Mesoporous Silica Nanoparticles: A Comprehensive Review on Synthesis and Recent Advances, *Pharmaceutics*, 2018, **10**(3), 118, DOI: 10.3390/pharmaceutics10030118.

17 M. J. Hollamby, D. Borisova, P. Brown, J. Eastoe, I. Grillo and D. Shchukin, Growth of Mesoporous Silica Nanoparticles Monitored by Time-Resolved Small-Angle Neutron Scattering, *Langmuir*, 2012, **28**(9), 4425–4433, DOI: 10.1021/la203097x.

18 C. T. Kresge, M. E. Leonowicz, W. J. Roth, J. C. Vartuli and J. S. Beck, Ordered Mesoporous Molecular Sieves Synthesized by a Liquid-Crystal Template Mechanism, *Nature*, 1992, **359**(6397), 710–712, DOI: 10.1038/359710a0.

19 F. Schüth, The Evolution of Ordered Mesoporous Materials, in *Studies in Surface Science and Catalysis*, ed. O. Terasaki, Mesoporous Crystals and Related Nano-Structured Materials, Elsevier, 2004, vol. 148, pp 1–13, DOI: 10.1016/S0167-2991(04)80190-3.

20 D. Zhao, J. Feng, Q. Huo, N. Melosh, G. H. Fredrickson, B. F. Chmelka and G. D. Stucky, Triblock Copolymer Syntheses of Mesoporous Silica with Periodic 50 to 300 Angstrom Pores, *Science*, 1998, **279**(5350), 548–552, DOI: 10.1126/science.279.5350.548.

21 Y. Lu, H. Fan, A. Stump, T. L. Ward, T. Rieker and C. J. Brinker, Aerosol-Assisted Self-Assembly of Mesostructured Spherical Nanoparticles, *Nature*, 1999, **398**(6724), 223–226, DOI: 10.1038/18410.

22 M. Vallet-Regi, A. Rámila, R. P. del Real and J. Pérez-Pariente, A New Property of MCM-41: Drug Delivery System, *Chem. Mater.*, 2001, **13**(2), 308–311, DOI: 10.1021/cm0011559.

23 D. Shen, J. Yang, X. Li, L. Zhou, R. Zhang, W. Li, L. Chen, R. Wang, F. Zhang and D. Zhao, Biphase Stratification Approach to Three-Dimensional Dendritic Biodegradable Mesoporous Silica Nanospheres, *Nano Lett.*, 2014, **14**(2), 923–932, DOI: 10.1021/nl404316v.

24 C. Kim, S. Yoon and J. H. Lee, Facile Large-Scale Synthesis of Mesoporous Silica Nanoparticles at Room Temperature in a Monophasic System with Fine Size Control, *Microporous Mesoporous Mater.*, 2019, **288**, 109595, DOI: 10.1016/j.micromeso.2019.109595.

25 T.-W. Kim, P.-W. Chung and V. S.-Y. Lin, Facile Synthesis of Monodisperse Spherical MCM-48 Mesoporous Silica Nanoparticles with Controlled Particle Size, *Chem. Mater.*, 2010, **22**(17), 5093–5104, DOI: 10.1021/cm1017344.

26 A. Noureddine, A. Maestas-Olguin, L. Tang, J. I. Corman-Hijar, M. Olewine, J. A. Krawchuck, J. Tsala Ebode, C. Edeh, C. Dang, O. A. Negrete, J. Watt, T. Howard, E. N. Coker, J. Guo and C. J. Brinker, Future of Mesoporous Silica Nanoparticles in Nanomedicine: Protocol for Reproducible Synthesis, Characterization, Lipid Coating, and Loading of Therapeutics (Chemotherapeutic, Proteins, siRNA and mRNA), *ACS Nano*, 2023, **17**(17), 16308–16325, DOI: 10.1021/acsnano.3c07621.

27 Machineagency/Science_jubilee, 2023, https://github.com/machineagency/science_jubilee, (accessed 2024-02-05).

28 S. Vasquez, H. Twigg-Smith, J. Tran O'Leary and N. Peek, Jubilee: An Extensible Machine for Multi-Tool Fabrication, in *Proceedings of the 2020 CHI Conference on Human Factors in Computing Systems; CHI '20*, Association for Computing Machinery, New York, NY, USA, 2020, pp 1–13, DOI: 10.1145/3313831.3376425.

29 N. Yoshikawa, K. Darvish, M. G. Vakili, A. Garg and A. Aspuru-Guzik, Digital Pipette: Open Hardware for

Liquid Transfer in Self-Driving Laboratories, *Digit. Discov.*, 2023, **2**(6), 1745–1751, DOI: 10.1039/D3DD00115F.

30 P. A. Beaucage and T. B. Martin, The Autonomous Formulation Laboratory: An Open Liquid Handling Platform for Formulation Discovery Using X-Ray and Neutron Scattering, *Chem. Mater.*, 2023, **35**(3), 846–852, DOI: 10.1021/acs.chemmater.2c03118.

31 B. Pelkie, S. Baird, E. Aissi, K. Aspuru-Takata, Y. Cao, J. H. Chang, K. Gambhir, W. S. Hale, L. Hao, C. Hattrick, J. Hein, D. Luo, O. Melville, M. Ngan, L. L. B. Nyeland, N. Peek, M. Politi, E. E. Rajkumar, A. Siemenn, B. Subbaraman, S. Vasquez, J. Watchorn, W. Zhang, R. Ziskason, L. Pozzo, T. Buonassisi and T. Vegge, Democratizing Self-Driving Labs through User-Developed Automation Infrastructure, *ChemRxiv*, 2025, DOI: 10.26434/chemrxiv-2025-zhkrf.

32 M. Zaki, C. Prinz and B. Ruehle, A Self-Driving Lab for Nano- and Advanced Materials Synthesis, *ACS Nano*, 2025, **19**(9), 9029–9041, DOI: 10.1021/acsnano.4c17504.

33 Jubilee, https://jubilee3d.com/index.php?title=Main_Page, (accessed 2025-05-13).

34 Science Jubilee — Science Jubilee 0.3.2.post1.dev170+g0ee6bd1 documentation, https://science-jubilee.readthedocs.io/en/latest/index.html (accessed 2025-06-02).

35 S. I. M, The Distribution of Points in a Cube and the Approximate Evaluation of Integrals, *USSR Comput. Math. Math. Phys.*, 1967, **7**, 86–112.

36 Sobol — SciPy v1.15.3 Manual, https://docs.scipy.org/doc/scipy/reference/generated/scipy.stats.qmc.Sobol.html#re15be05a07a0-1 (accessed 2025-06-02).

37 C. G. Tan, B. D. Bowen and N. Epstein, Production of Monodisperse Colloidal Silica Spheres: Effect of Temperature, *J. Colloid Interface Sci.*, 1987, **118**(1), 290–293, DOI: 10.1016/0021-9797(87)90458-9.

38 J.-M. Zárate-Reyes, E. Flores-Romero and J.-C. Cheang-Wong, Systematic Preparation of High-Quality Colloidal Silica Particles by Sol–Gel Synthesis Using Reagents at Low Temperature, *Int. J. Appl. Glass Sci.*, 2022, **13**(1), 54–62, DOI: 10.1111/ijag.16108.

39 Usnistgov/AFL-Automation, 2025, https://github.com/usnistgov/AFL-automation (accessed 2025-05-13).

40 Usnistgov/AFL-Hardware, 2024, https://github.com/usnistgov/AFL-hardware (accessed 2025-05-13).

41 Automation-Hardware/Cartridge Sample Holder for SAS Experiments/SAXS-USAXS Liquids 48 well plate holder at master pozzo-research-group/Automation-Hardware, https://github.com/pozzo-research-group/Automation-Hardware/tree/master/Cartridge%20Sample%20Holder%20for%20SAS%20Experiments/SAXS-USAXS%20Liquids%2048%20well%20plate%20holder (accessed 2025-05-05).

42 J. Ilavsky, F. Zhang, R. N. Andrews, I. Kuzmenko, P. R. Jemian, L. E. Levine and A. J. Allen, Development of Combined Microstructure and Structure Characterization Facility for in Situ and Operando Studies at the Advanced Photon Source, *J. Appl. Crystallogr.*, 2018, **51**(3), 867–882, DOI: 10.1107/S160057671800643X.

43 Automation-Hardware/Cartridge Sample Holder for SAS Experiments/SAXS-USAXS_AntonPaar_FlowCellHolder/USAXS_flow cell holder v5.stl at master pozzo-research-group/Automation-Hardware. GitHub, https://github.com/pozzo-research-group/Automation-Hardware/blob/master/Cartridge%20Sample%20Holder%20for%20SAS%20Experiments/SAXS-USAXS_AntonPaar_FlowCellHolder/USAXS_flow%20cell%20holder%20v5.stl (accessed 2025-05-05).

44 pozzo-research-group/automated-MSN-synthesis: Documentation and example code for forthcoming automated mesoporous silica nanoparticle synthesis paper, https://github.com/pozzo-research-group/automated-MSN-synthesis (accessed 2025-06-02).

45 G. Roberts, M.-P. Nieh, W. K. Ma and Q. Yang, Automated Structural Analysis of Small Angle Scattering Data from Common Nanoparticles via Machine Learning, *Digit. Discov.*, 2025, **4**, 1467–1477, DOI: 10.1039/D5DD00059A.

46 P. Tomaszewski, S. Yu, M. Borg and J. Rönnols, Machine Learning-Assisted Analysis of Small Angle X-Ray Scattering, in *2021 Swedish Workshop on Data Science (SweDS)*, 2021, pp 1–6, DOI: 10.1109/SweDS53855.2021.9638297.

47 R. K. Archibald, M. Doucet, T. Johnston, S. R. Young, E. Yang and W. T. Heller, Classifying and Analyzing Small-Angle Scattering Data Using Weighted k Nearest Neighbors Machine Learning Techniques, *J. Appl. Crystallogr.*, 2020, **53**(2), 326–334, DOI: 10.1107/S1600576720000552.

48 S. V. R. Akepati, N. Gupta and A. Jayaraman, Computational Reverse Engineering Analysis of the Scattering Experiment Method for Interpretation of 2D Small-Angle Scattering Profiles (CREASE-2D), *JACS Au*, 2024, **4**(4), 1570–1582, DOI: 10.1021/jacsau.4c00068.

49 Z. Ye, Z. Wu and A. Jayaraman, Computational Reverse Engineering Analysis for Scattering Experiments (CREASE) on Vesicles Assembled from Amphiphilic Macromolecular Solutions, *JACS Au*, 2021, **1**(11), 1925–1936, DOI: 10.1021/jacsau.1c00305.

50 K. Vaddi, H. T. Chiang and L. D. Pozzo, Autonomous Retrosynthesis of Gold Nanoparticles via Spectral Shape Matching, *Digit. Discov.*, 2022, **1**(4), 502–510.

51 V. Candela-Noguera, M. Alfonso, P. Amorós, E. Aznar, M. D. Marcos and R. Martínez-Máñez, In-Depth Study of Factors Affecting the Formation of MCM-41-Type Mesoporous Silica Nanoparticles, *Microporous Mesoporous Mater.*, 2024, **363**, 112840, DOI: 10.1016/j.micromeso.2023.112840.

52 SasView, https://sasview.github.io/(accessed 2025-05-12).

53 C. Giacomelli and R. Borsali, Disordered Phase and Self-Organization of Block Copolymer Systems, in *Soft Matter Characterization*, ed. R. Borsali and R. Pecora, Springer Netherlands, Dordrecht, 2008, pp 133–189, DOI: 10.1007/978-1-4020-4465-6_3.